

# Empirical Adaptive Wavelet Decomposition (EAWD): An adaptive decomposition for the variability analysis of observation time series in atmospheric science.

Olivier Delage<sup>1</sup>, Thierry Portafaix<sup>1</sup>, Hassan Bencherif<sup>1,2</sup>, Alain Bourdier<sup>3</sup>,  
Emma Lagracie<sup>1,4</sup>

<sup>1</sup> Laboratoire de l'Atmosphère et des Cyclones, (LACy, UMR 8105 CNRS, Université de la Réunion, Météo-France), Université de La Réunion, 97400 Saint-Denis de La Réunion, France

<sup>2</sup> School of Chemistry and Physics, University of KwaZulu-Natal, Westville, Durban 4041, South Africa

<sup>3</sup> Department of Physics and Astronomy, The University of New Mexico, Albuquerque, NM, USA

<sup>4</sup> École Nationale Supérieure des Techniques Avancées, Paris, France

*Correspondence to:* olivier.delage@univ-reunion.fr

**ABSTRACT.** Most observational data sequences in geophysics can be interpreted as resulting from the interaction of several physical processes at several time and space scales. In consequence, measurement time series often have characteristics of non-linearity and non-stationarity and thereby exhibit strong fluctuations at different time-scales. The application of decomposition methods is an important step in the analysis of time series variability, allowing patterns and behaviour to be extracted as components providing insight into the mechanisms producing the time series. This study introduces Empirical Adaptive Wavelet Decomposition (EAWD), a new adaptive method for decomposing non-linear and non-stationary time series into multiple empirical modes with non-overlapping spectral contents. The method takes its origin from the coupling of two widely used decomposition techniques: empirical mode decomposition (EMD) and empirical wavelet transformation (EWT). It thus combines the advantages of both methods and can be interpreted as an optimization of EMD. Here, through experimental time series applications, EAWD is shown to accurately retrieve different physically meaningful components concealed in the original signal.

**KEY-WORDS:** Variability Analysis, Complex Dynamics, Adaptive Filtering, Empirical Mode Decomposition (EMD), Empirical Wavelet Transformation (EWT), Non-Linear and Non-Stationary time series, Wavelet, Atmospheric observation.

## 1 Introduction

Most geophysical systems are complex and the variability of the corresponding observation time series is characterized by large fluctuations at different time scales. To analyse these fluctuations and the associated multi-scale dynamics, some specific methods have been developed. Empirical mode decomposition (EMD) is part of a more general signal processing method called the Hilbert-Huang transform (HUANG et al., 1998) and consists in decomposing a signal in a self-adaptive way, into a sum of oscillating components named IMFs (Intrinsic Mode Functions). Each IMF captures the repeating signal behaviour at some particular time scale. Like the wavelet transform, the EMD techniques reduce a time signal to a set of basis signals; unlike the wavelet transform, the basic functions are derived from the signal itself. The main advantages of the EMD method are that it is fully adaptive, data-driven and, indeed, close to the observed dynamics. As the EMD acts as a bank of bandpass filters (FLANDRIN et al., 2004), the main limiting factor is the frequency resolution, which may give rise to the mode mixing phenomenon where the spectral contents of some IMFs overlap each other (GAO et al., 2008).

Although several techniques exist to overcome this problem (FOSSO et al., 2017, DELAGE et al., 2019), Gilles (2013) proposed an alternative one entitled “Empirical Wavelet Transform” (EWT), which builds a wavelet filter bank from the segmentation of the original signal’s Fourier spectrum. This approach is similar to that used in the construction of both Littlewood-Paley and Meyers wavelets (MEYER, 1997). The heart of the EWT method is the segmentation of the Fourier spectrum based on the detection of local maxima, in order to obtain a set of non-overlapping segments. Because it is linked to the Fourier spectrum, the frequency resolution provided by the EWT is higher than that provided by the EMD and therefore allows the mode mixing problem to be overcome. Although the EWT technique enables detection of the relevant frequencies involved in the original time series fluctuations, such a technique does not enable the detected frequencies to be associated to a specific mode of variability as EMD does. Because the EMD is closer to the observed dynamics than EWT, in the present work, we developed a new approach called EAWD (Empirical Adaptive Wavelet Decomposition) based on the coupling of the EMD and EWT techniques. We use the spectral content of the IMFs retrieved by EMD to optimize the segmentation of the

original time series Fourier spectrum required by EWT. This document is structured around four sections. The first section is devoted to the EMD and EWT techniques. In the second one, the new adaptive decomposition EAWD is described and explains why such a method can be considered as an optimization of the EMD. In the third section, two observation time series are analysed by using EMD and EAWD techniques and the corresponding results are presented. Finally, the results obtained respectively with the EMD and EAWD techniques are compared and discussed.

## 2-The existing approaches.

### 2.1 Empirical Mode Decomposition (EMD).

In 1998, HUANG et al. proposed an original method called Empirical Mode Decomposition (EMD), which adaptively decomposes any signal into oscillatory contributions. In a nutshell, EMD can be summarized as an iterative method where the signal is considered as the superimposition of high and low-frequency oscillations. At each iteration, high-frequency oscillation components are separated from the low-frequency oscillations, then reinjected as a new signal in the following iteration. The EMD is thus directly controlled by the signal itself and not by some filtering operations as in the wavelet decomposition. More precisely, the decomposition is carried out at the scale of local oscillations, the low-frequency modes being obtained as the mean value of an upper and a lower envelope computed as cubic spline interpolations between maxima and minima, respectively. By subtracting this component from the original signal, we obtain what is called an ‘‘Intrinsic Mode Function’’ (IMF). The procedure is then applied to the low-frequency part as a new signal to be decomposed and successive oscillatory components are iteratively extracted from the original signal. The original time series  $x(t)$  can finally be expressed as the sum of a finite number,  $N$ , of IMFs and a residual term,  $R$ , which cannot be assimilated to an oscillation.

$$x(t) = \sum_{i=1}^N IMF_i(t) + R(t) \quad (1)$$

The interesting fact about this algorithm is that it is highly adaptable and is able to extract the non-stationary part of the original signal. However, in practice, the EMD technique presents some limiting factors. For example, some problems appear when a certain amount of noise is present in the signal. To deal with this problem, (WU and WANG, 2009) introduced an EMD optimization entitled Ensemble Empirical Mode Decomposition (EEMD). The principle behind EEMD is to average the modes obtained by EMD after several realizations of Gaussian white noise that are added to the original signal. This approach seems to stabilize the decomposition obtained.

### 2.2 Wavelet approaches.

Wavelets are commonly used to analyse the variability of a signal. In the temporal domain, a wavelet basis is defined as the mother wavelet  $\psi$  of zero-mean, dilated with a parameter  $s > 0$  and translated by  $u \in \mathbb{R}$ :

$$\psi_{u,s}(t) = \frac{1}{\sqrt{s}} \psi\left(\frac{t-u}{s}\right). \quad (2)$$

For the wavelet decomposition of a time series  $x(t)$ , the most widely used case is the dyadic one,  $s=2^j$ . Then the wavelet decomposition of  $x$  is obtained by computing the inner products  $W_x(k, j)$  as:

$$W_x(k, j) = \langle x, \psi_{k,j} \rangle \text{ with } \psi_{k,j}(t) = \frac{1}{\sqrt{2^j}} \psi\left(\frac{t-k}{2^j}\right), k \in \mathbb{Z} \quad (3)$$

where  $j$  represents the resolution level. The decomposition is then similar to a multiresolution analysis carrying out successive projections of  $x$  on a sequence of nested subspaces  $V_j \in L^2(\mathbb{R})$   $j = [0, n]$ , which leads to increasingly coarse approximations of  $x$  as  $j$  increases. The difference between two successive approximations, resulting from projections of  $x$  on  $V_{j-1}$  and  $V_j$ , contains the information of ‘‘details’’, which existed at the scale  $2^{j-1}$  but which is lost at the scale  $2^j$ . This information is contained in the subspace  $W_j$  orthogonal to  $V_j$  such that  $V_{j-1} = V_j \oplus W_j$ , where  $\oplus$  denotes the direct sum of vector subspaces. The orthogonal projection of  $x$  on  $W_j$  gives the information of ‘‘details’’ at the resolution level  $j$ . Wavelets  $\{\psi_{k,j}(t), k \in \mathbb{Z}\}$  form a basis of  $W_j$ . According to the definition of a multiresolution analysis, there exists a function  $\varphi(t)$ , called a scaling function, such that  $\{\varphi(t-k), k \in \mathbb{Z}\}$  form a basis of  $V_0$  corresponding to the coarsest approximation of  $x$ . The reconstruction of  $x$  is obtained from:

$$x(t) = \langle x(t), \varphi(t) \rangle \cdot \varphi(t) + \sum_{j=1}^N \langle x(t), \psi_{k,j}(t) \rangle \cdot \psi_{k,j}(t) \quad (4)$$

1 where  $\langle \cdot \rangle$  represents the inner products. The approximation coefficients corresponding to the coarsest resolution  
 2 level are given by  $\langle x, \varphi \rangle$  and the detail coefficients corresponding to the successively decreasing resolution level  
 3  $\Delta s_j = \Delta s_{j-1}/2$  are given by  $\langle x, \psi_{k,j} \rangle$  as follows:

$$4 \quad \langle x(t), \varphi(t) \rangle = \int x(\tau) \overline{\varphi(\tau - t)} d\tau; \quad \langle x(t), \psi_{k,j}(t) \rangle = \int x(\tau) \overline{\psi_{k,j}(\tau - t)} d\tau \quad (5)$$

### 6 2.3 Empirical wavelets- The Empirical Wavelet Transformation (EWT).

7  
 8 The essence of EMD is that the functions into which a signal is decomposed are all in the time domain of, and  
 9 have the same length as, the original signal, allowing time-varying frequencies to be preserved. In this context,  
 10 Rilling et al. (2004) described the EMD as behaving as a dyadic filter bank like those involved in the  
 11 multiresolution analysis. This can be interpreted as the presence of several filters of overlapping frequency content  
 12 that may give rise to the mode mixing phenomenon, which is defined as a single IMF consisting either of widely  
 13 disparate scales, or of similar scales residing in different IMFs. In that case, the spectral contents of some IMFs  
 14 overlap each other. To overcome this problem, Gilles (2013) proposed an alternative named the ‘‘Empirical  
 15 Wavelet Transform’’ (EWT). As the EMD technique acts as a filter bank in the spectral domain, so the method  
 16 proposed by Gilles (2013) designs an appropriate wavelet filter bank from the segmentation of the original signal’s  
 17 Fourier spectrum. The Fourier support  $[0, \pi]$  is segmented into N contiguous segments denoted  $\Delta_n = [\omega_{n-1}, \omega_n]$ .  
 18 The filter bank (MEYER, 1997; JAFFARD et al., 2001) is defined by the empirical scaling function and the  
 19 empirical wavelets on each  $\Delta_n$  through Equations 6 and 7, respectively:

$$20 \quad \widehat{\phi}_n(\omega) = \begin{cases} 1 & \text{if } |\omega| \leq (1 - \gamma)\omega_n \\ \cos \left[ \frac{\pi}{2} \beta \left( \frac{1}{2\gamma\omega_n} (|\omega| - (1 - \gamma)\omega_n) \right) \right] & \text{if } (1 - \gamma)\omega_n \leq |\omega| \leq (1 + \gamma)\omega_n \\ 0 & \text{otherwise} \end{cases} \quad (6)$$

$$21 \quad \widehat{\psi}_n(\omega) = \begin{cases} 1 & \text{if } (1 + \gamma)\omega_n \leq |\omega| \leq (1 - \gamma)\omega_{n+1} \\ \cos \left[ \frac{\pi}{2} \beta \left( \frac{1}{2\gamma\omega_{n+1}} (|\omega| - (1 - \gamma)\omega_{n+1}) \right) \right] & \text{if } (1 - \gamma)\omega_{n+1} \leq |\omega| \leq (1 + \gamma)\omega_{n+1} \\ \sin \left[ \frac{\pi}{2} \beta \left( \frac{1}{2\gamma\omega_n} (|\omega| - (1 - \gamma)\omega_n) \right) \right] & \text{if } (1 - \gamma)\omega_n \leq |\omega| \leq (1 + \gamma)\omega_n \\ 0 & \text{otherwise} \end{cases} \quad (7)$$

23 The function  $\beta(x)$  is an arbitrary  $C^k([0,1])$  function defined as:

$$24 \quad \beta(x) = \begin{cases} 0 & \text{if } x \leq 0 \\ \beta(x) + \beta(1 - x) = 1 \quad \forall x \in [0,1] \\ 1 & \text{if } x \geq 1 \end{cases} \quad (8)$$

25 Many functions satisfy this property and the one most used in the literature (DAUBECHIES, 1992) is:

$$26 \quad \beta(x) = x^4(35 - 84x + 70x^2 - 20x^3) \quad (9)$$

27  
 28 The parameter  $\gamma$  is chosen to satisfy the following criterion:

$$29 \quad \gamma < \text{Min}_n \left( \frac{\omega_{n+1} - \omega_n}{\omega_{n+1} + \omega_n} \right) \quad (10)$$

30  
 31 The details and approximation coefficients are calculated by using Eqs. 6 and 7 and are respectively given by inner  
 32 products with the empirical wavelets  $\psi_n$  and the scaling function  $\phi_1$

$$33 \quad W_x(n, t) = \langle x(t), \psi_n \rangle = \text{IFFT}(X(\omega) \cdot \overline{\widehat{\psi}_n(\omega)}) \quad (11)$$

$$34 \quad W_x(1, t) = \langle x(t), \phi_1 \rangle = \text{IFFT}(X(\omega) \cdot \overline{\widehat{\phi}_1(\omega)}) \quad (12)$$

35  
 36 where X is the Fourier transform of the original signal x,  $\overline{\phantom{x}}$  represents the complex conjugate, and IFFT represents the  
 37 inverse Fourier transform, and  $\psi_n$  and  $\phi_1$  are the results of the inverse Fourier transforms of  $\widehat{\psi}_n$  and  $\widehat{\phi}_1$ , respectively.  
 38

1 The heart of the empirical wavelet transform is the segmentation of the original signal's Fourier spectrum. In order to  
 2 obtain a set of non-overlapping segments, the Fourier spectrum local maxima are detected. Each segment is centred around  
 3 a group of one or more local maxima. The limit between two contiguous segments, each of them characterized by a group  
 4 of local maxima, is determined as the local minimum closest to the midpoint between the two local maxima groups. Many  
 5 of the detected local maxima are irrelevant as their contributions to the variability of the original time series are negligible.  
 6 Selecting the relevant local maxima requires the setting of a threshold, which is not always possible.  
 7

### 8 3 The Empirical Adaptive Wavelet Decomposition (EAWD). 9

10 The EMD enables an observation data sequence to be decomposed into multiple empirical modes of variability, each of  
 11 them reflecting the observed dynamics at a specific time scale. However, in some cases, the frequency resolution provided  
 12 by EMD does not allow IMFs with disjoint spectral support to be retrieved.

13 The adaptive wavelet transform (EWT) is one of several interesting methods pursuing the same goal as EMD, which allows  
 14 the mode-mixing problem to be overcome. This method relies on robust pre-processing for peak detection, then performs  
 15 original signal Fourier spectrum segmentation based on detected maxima, and constructs a corresponding wavelet filter  
 16 bank.

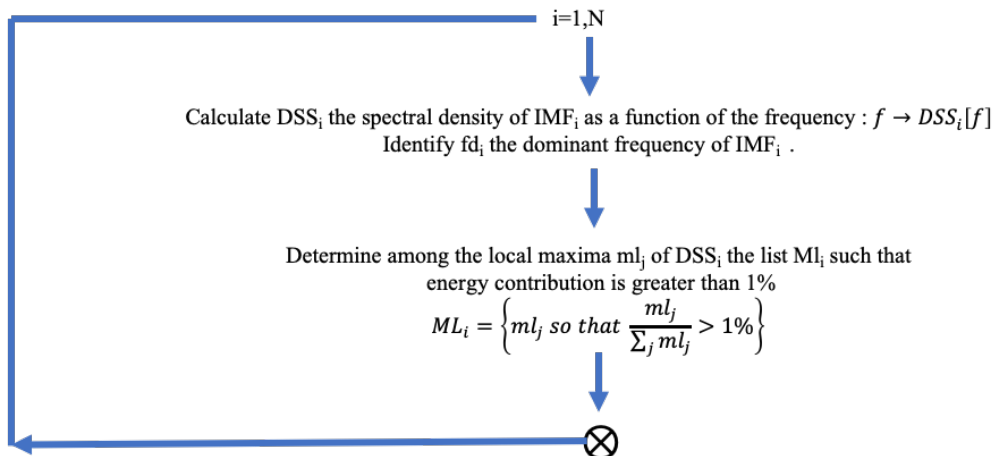
17 The main idea of the proposed EAWD method is to combine EMD and EWT techniques by setting non-overlapping groups  
 18 of local maxima from the spectral contents of the IMFs returned by the EMD technique.  
 19

20 Each IMF local maxima group will be associated with a segment of the original signal Fourier spectrum segmentation. The  
 21 boundaries of each of these segments will be set as the local minima located between local maxima groups of two  
 22 consecutive IMFs. As the EMD acts like a bank of dyadic band-pass filters, the result of each of these filters, in the  
 23 frequency domain, is composed of a set of local maxima relative to a specific timescale in which the resolution is divided  
 24 by two in comparison with the timescale immediately above it. Considering that a timescale is characterized by the set of  
 25 values in the range of  $[2^n, 2^{n+1}]$ , to carry out a segmentation of the Fourier spectrum, it is necessary to distribute the local  
 26 maxima groups relatively to a grid  $[2^i, 2^{i+1}]$ ,  $i \in [2, J]$  with  $J = \text{int} \left( \frac{\log(N)}{\log(2)} \right) - 1$ , where N is the size of the original time  
 27 series.

28 The proposed Fourier spectrum segmentation algorithm is based on two main points:

- 29 1- The spectrum of two consecutive IMFs contains at most two different dominant frequencies. Relative to the  
 30 spectral content of an IMF, the frequency with the greatest spectral density is called the dominant frequency.
- 31 2- The local maxima list of the spectra of two consecutive IMFs is subdivided into three groups: the local maxima  
 32 belonging to IMF<sub>i</sub> spectrum, ML1; the local maxima belonging to the intersection of IMF<sub>i</sub> and IMF<sub>i+1</sub> spectra,  
 33 MLINTER; and the local maxima belonging to IMF<sub>i+1</sub> spectrum, ML2.  
 34

35 The proposed EAWD algorithm is composed of three steps as described in the diagrams below (see Figure 1, Figure 2,  
 36 Figure 3).  
 37



38  
 39  
 40 **Figure 1:** Estimation of the spectral density for each IMF spectrum and selection of significant local maxima whose  
 41 energy contribution > 1%.

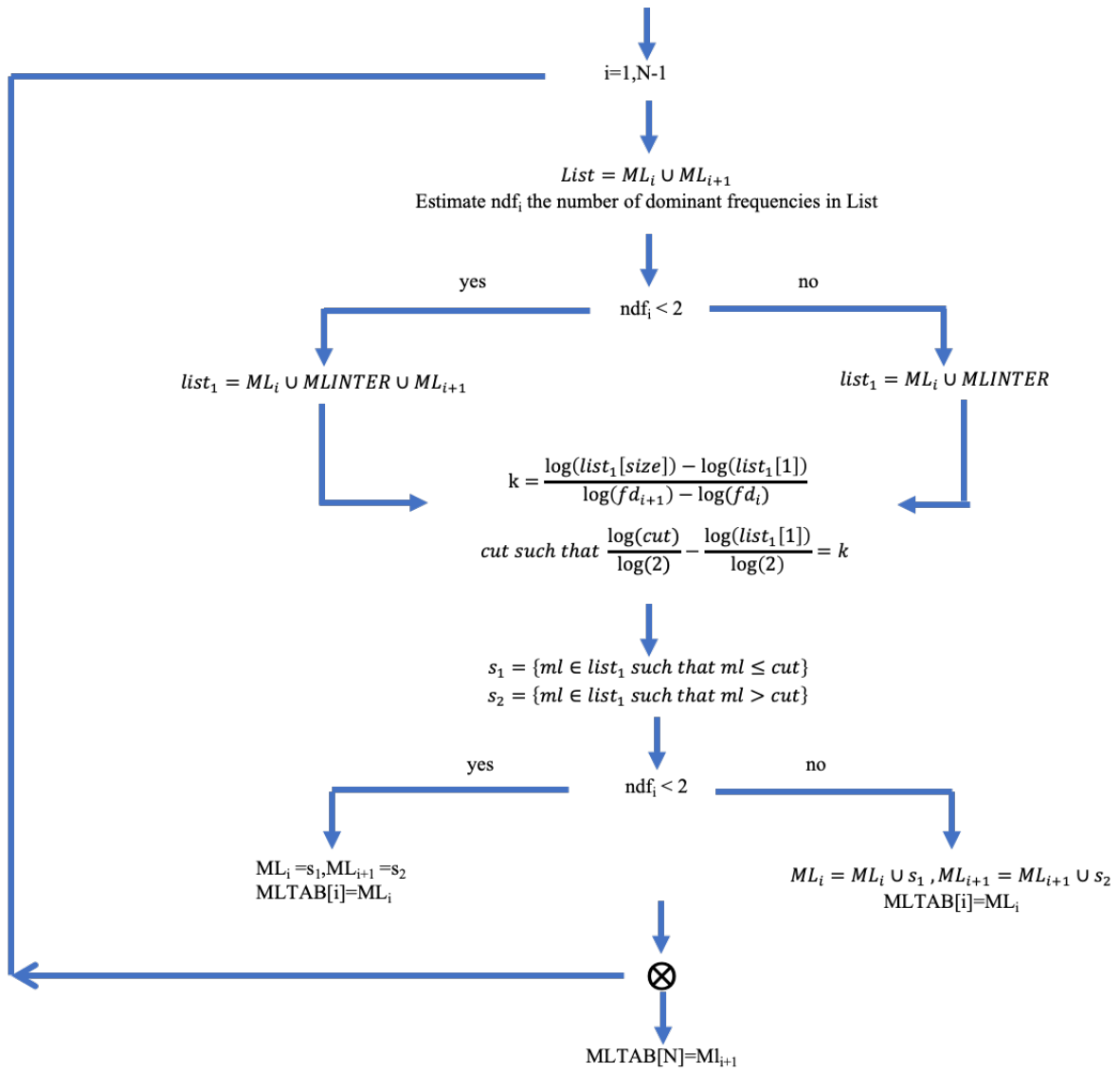


**Figure 2:** Calculation of the matrix MLTAB. Each row of MLTAB contains the list of significant local maxima present in the spectrum of an IMF. The rows of MLTAB have no common elements and therefore MLTAB can be seen as a set of non-overlapping local maxima groups and represents a segmentation of the original signal Fourier spectrum.

“size” represents the length of list1 and “cut” is the boundary between two consecutive local maxima groups  $ML_i$  and  $ML_{i+1}$ .

The parameter  $k$  can be interpreted as the ratio between the number of scales contained in list1 and the number of scales in the interval  $[fd_i, fd_{i+1}]$  of two consecutive dominant frequencies.

1  
2  
3  
4  
5  
6  
7  
8  
9  
10  
11  
12  
13

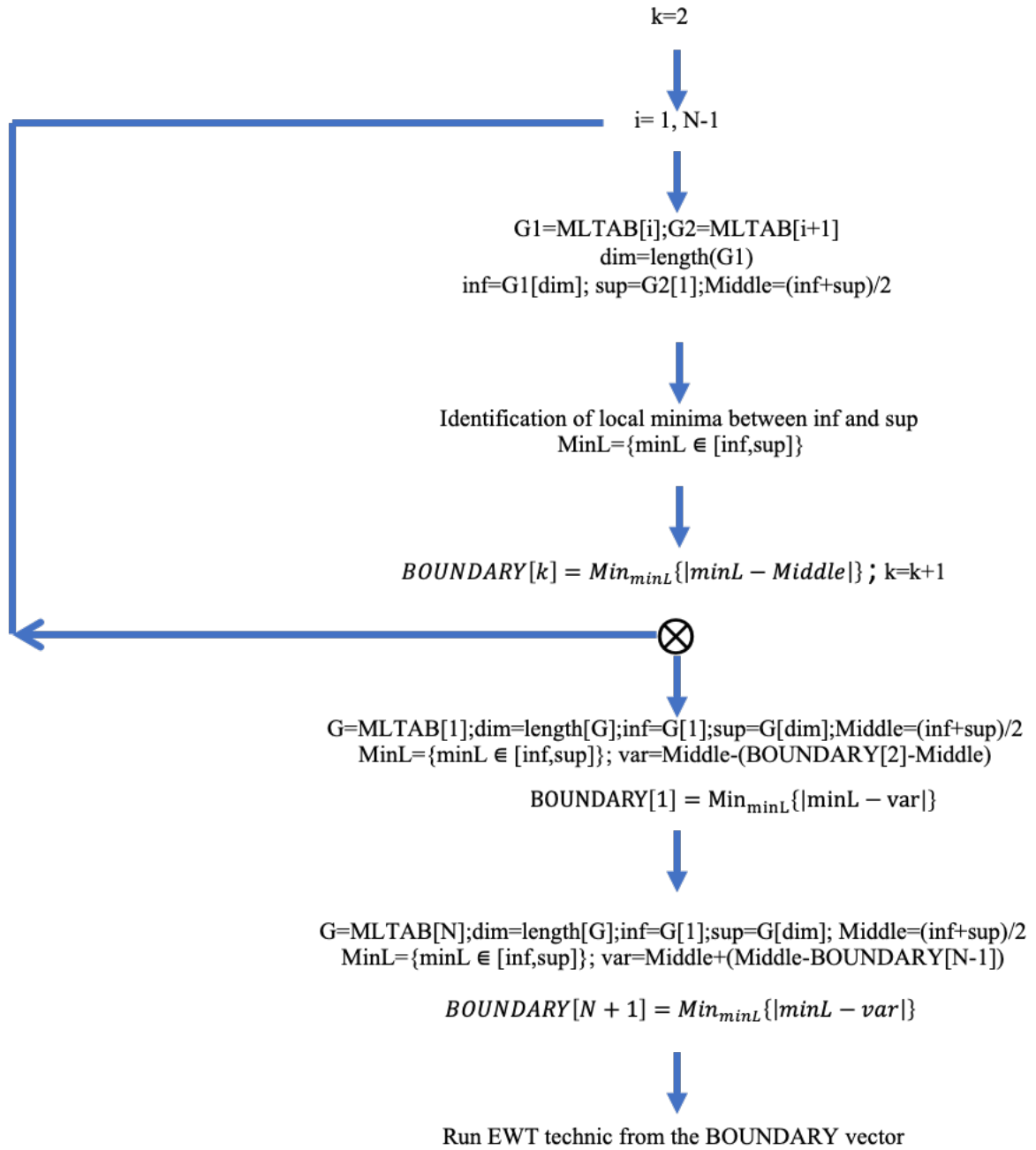


**Figure 3:** Calculation of the BOUNDARY vector representing the boundaries between the local maxima groups contained in the matrix MLTAB. The EWT technique is run from BOUNDARY.

#### 4 Time series analysis and results.

The EMD and EAWD techniques presented above have been applied to two experimental time series of observations. The first time-series was a series of monthly Total Columns of Ozone (TCO) in Dobson units, recorded over 41 years, from January 1979 to December 2019, by a SAOZ (Zenithal Observation Analysis System) spectrometer on the Moufia University Campus, Saint-Denis, Reunion Island (21°S, 55.5°E).

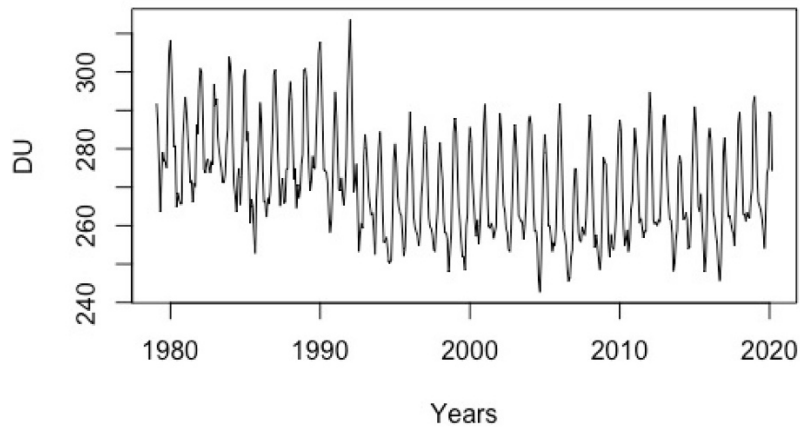
This TCO time series was elaborated by merging satellite data (OMI and TOMS) and ground-based observations recorded by a SAOZ spectrometer (Pommereau and Goutail, 1988) installed at Saint Denis, Réunion Island in 1993. The method used for merging satellite and ground data to obtain a homogeneous series is explained in Pastel et al., 2014.

Despite its low abundance, ozone plays an important role in the Earth's atmosphere. It is mainly produced in the tropical stratosphere and transported to higher latitudes by the large-scale circulation called the Brewer-Dobson circulation. In the stratosphere, ozone acts like a filter and prevents incident solar ultraviolet (UV) radiation from reaching the ground, thus

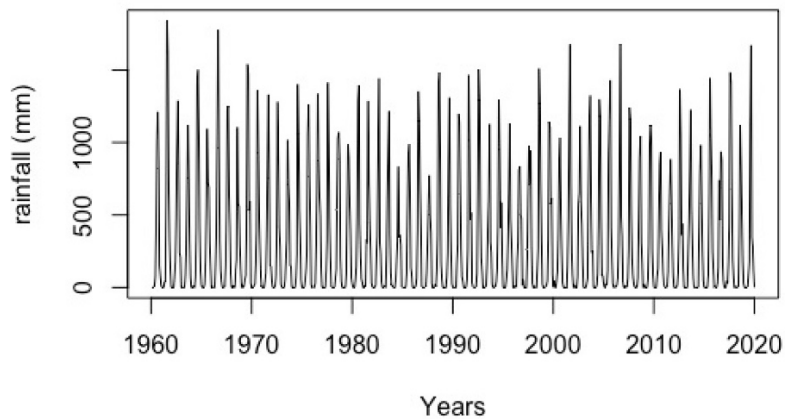
1 protecting the biosphere. The significant depletion of the ozone layer since the late 1970s has revealed the importance of  
 2 ozone in the climate system and the associated environmental and health risks. The TCO is a parameter that measures the  
 3 abundance of ozone over a given location. It is given in Dobson Units (DU) and consists of ~90% stratospheric ozone and  
 4 ~10% tropospheric ozone.

5 The second time-series comprised 57 years of monthly rainfall measurements recorded at Conakry (Guinea)  
 6 meteorological station from 1961 to 2017.

7 The resulting original time series of total ozone columns and rainfall measurements are displayed in Figure 4 and  
 8 Figure 5, respectively.



9  
 10 **Figure 4:** Monthly time-series of total ozone columns in Dobson Units (DU) over Réunion Island from 1979 to 2019.  
 11 Time axis is expressed in years.  
 12



13  
 14 **Figure 5:** Monthly Rainfall records time series recorded at Conakry (Guinea) from 1960 to 2019. Time axis is  
 15 expressed in years.

16 Very often, noise is present in the original time series. To deal with this problem, the authors suggest computing  
 17 an Ensemble Empirical Mode decomposition (EEMD) (Z.Wu, NE Wang, 2009). This approach seems to reduce  
 18 the noise present in the original signal. Generally, some of the IMFs returned by the EEMD technique present poor  
 19 correlations with the original signal and therefore make a weak contribution in the variability of the original series.  
 20 Such IMFs are qualified as irrelevant. Relevant IMFs are discriminated from the irrelevant ones by means of two  
 21 criteria. The first of these criteria uses Pearson's correlation to estimate the degree of correlation of each IMF with  
 22 the original signal by setting a threshold. A threshold commonly used in the literature (Ayenu-Prah et al., 2010)  
 23 can be expressed as:  
 24

25  
 26  
 27 
$$\tau = \frac{\max(\text{Cor}(IMF_i, x))}{(10 * \max(\text{Cor}(IMF_i, x))) - 3} \quad (13)$$

In Equation (13),  $Cor(IMF_i, x)$  stands for the Pearson's correlation coefficient between the  $i^{th}$  IMF and the original signal  $x(t)$ , i.e.:

$$Cor(IMF_i, x) = \frac{Cov(IMF_i, x)}{sd(IMF_i) * sd(x)} \quad (14)$$

where  $sd$  represents the standard deviation and  $cov(.,.)$  the covariance.

The second criterion determines the energy contribution of each IMF compared to the energy contained in the original signal. The energy contribution of each IMF is calculated as a percentage as follows:

$$CENR = \left( \frac{E_i}{E_x} \right) * 100 = \frac{var(IMF_i)}{var(x - \bar{x})} * 100 \quad (15)$$

where  $E_i = \sum_1^N IMF_i^2(t) = var(IMF_i)$  because each IMF is a zero-mean function by construction.  $E_x = \sum_1^N x^2(t) = var(x - \bar{x})$ .

The threshold set for this second criterion is 1%.

IMFs having a degree of correlation less than  $\tau$  and for which the energy contribution is less than 1% are said to be irrelevant. The irrelevant IMFs are added to the residual mode  $R$  returned by the EEMD to form the trend of the original signal. For such IMFs to be part of the trend of the observed dynamics, they must not be too oscillating and are therefore contiguous to the residue.

When EEMD was applied to La Reunion TCO time series presented in Figure 4, seven IMFs were found in addition to the residual mode. Taking account of the selection procedure mentioned above, the first five of the seven IMFs initially identified were relevant and IMFs 6 and 7 were added to the residual mode. Results are displayed in Figure 6 below.

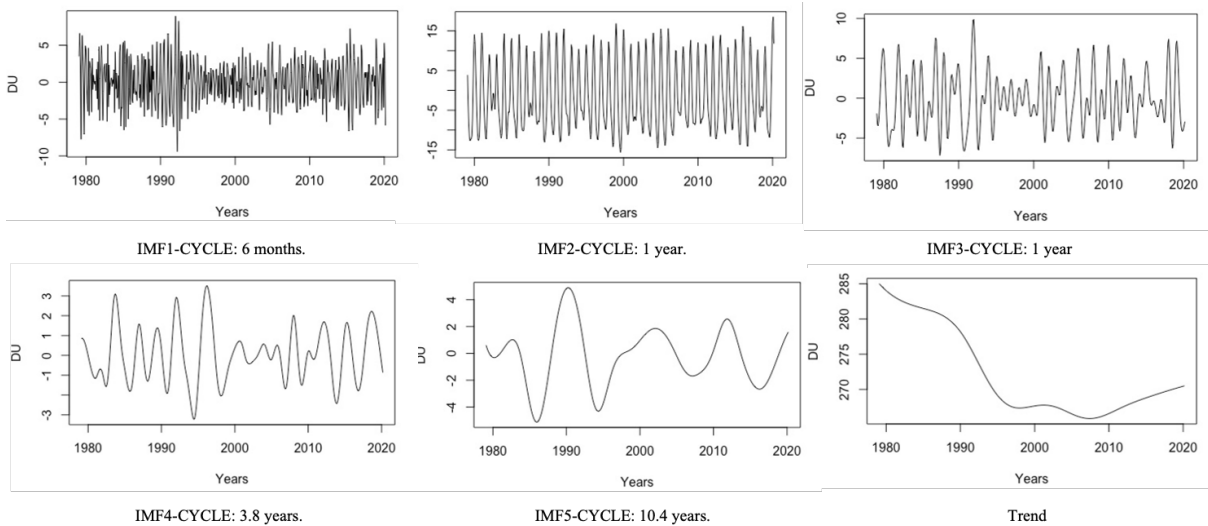
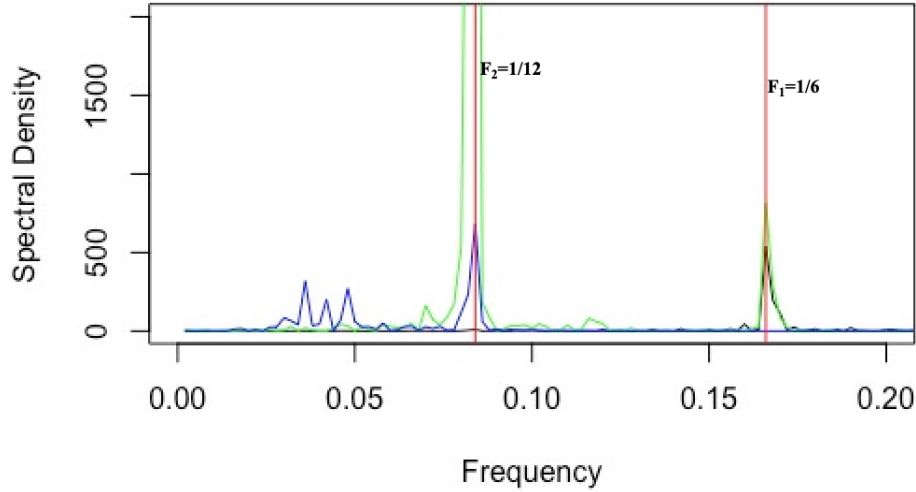


**Figure 6:** Relevant IMFs and Trend from the EEMD applied to time series of La Reunion total columns of ozone from 1979 to 2019.

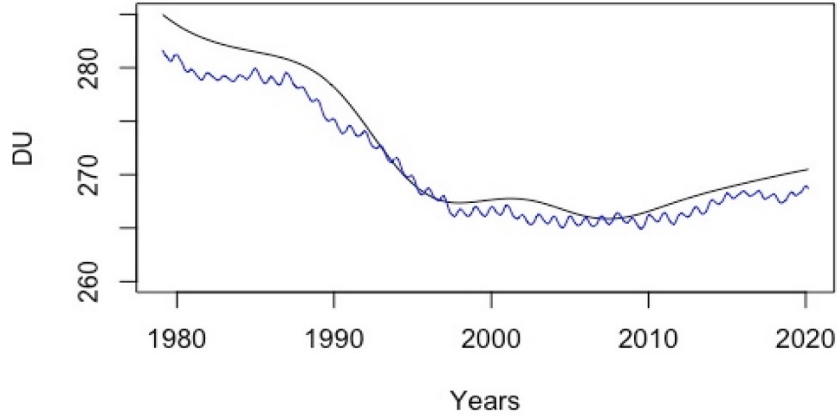
For each IMF, the cycle defined as the period associated with the dominant frequency is specified. Mode mixing occurs in  $IMF_2$  and  $IMF_3$  as they have the same 1year oscillation cycle. As shown in Figure 7,  $IMF_2$  spectrum contains  $F_1=1/6$  and  $F_2=1/12$  frequencies and  $F_2$  is contained in both  $IMF_2$  and  $IMF_3$ .





1  
2  
3 **Figure 7:** TCO IMF<sub>1</sub> (black line), IMF<sub>2</sub> (green line) and IMF<sub>3</sub> (blue line) spectral contents.

4 To estimate the accuracy of the residual returned by the EEMD, it is compared with the trend of the original signal obtained  
5 from a moving window having a size set at the maximum of the relevant IMF cycles i.e. 125 months (10.4 years).



6  
7  
8 **Figure 8:** Trend obtained from the EEMD technique (black curve). The trend of the original signal obtained from a  
9 moving window (blue curve) with a 125-month size (i.e. 10.4 years).  
10

11 The accuracy of the residual, R, returned by the EEMD and compared with the trend of the original signal by using a  
12 moving window, Tmb was estimated using the following expression:

13 
$$Pr_{EEMD} = \sqrt{\frac{\sum_{i=1}^N (R(i) - \overline{Tmb(i)})^2 / N}{Tmb}} * 100 = 0.7\%$$
 (16)  
14

15 where N is the original time-series length and  $\bar{\cdot}$  represents the mean operator.

16 To overcome the mixing mode occurring in IMFs 2 and 3 returned by the EEMD technique, we applied the EAWD  
17 technique to the Reunion TCO time-series. The results obtained with EAWD are displayed in Figure 9 below.  
18

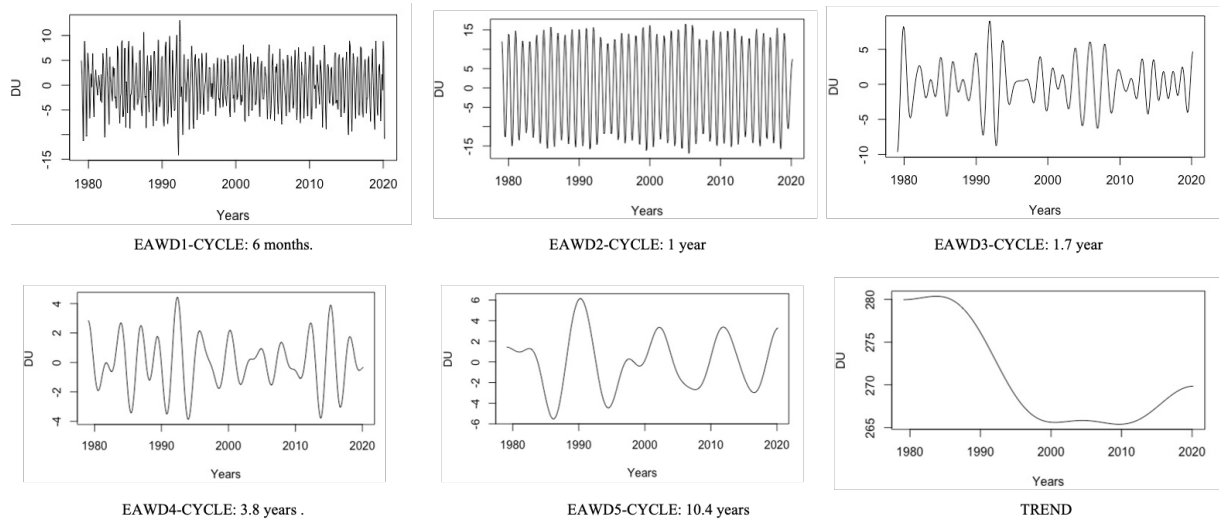


**Figure 9:** Réunion total ozone time-series EAWD decomposition results.

As shown in Figure 10 below, the 6 month and 1 year cycles relating respectively to EAWD1 and EAWD2 are correctly separated and the mode mixing occurring in the EEMD results has been removed.

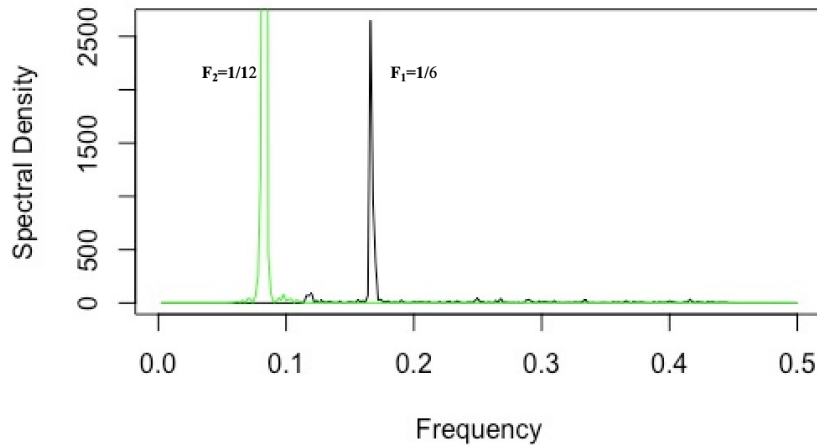


**Figure 10:** TCO EAWD<sub>1</sub> (black line), EAWD<sub>2</sub> (green line) spectral contents.

Similarly, the accuracy of the residual returned by the EAWD technique was estimated and compared to that returned by the EEMD.

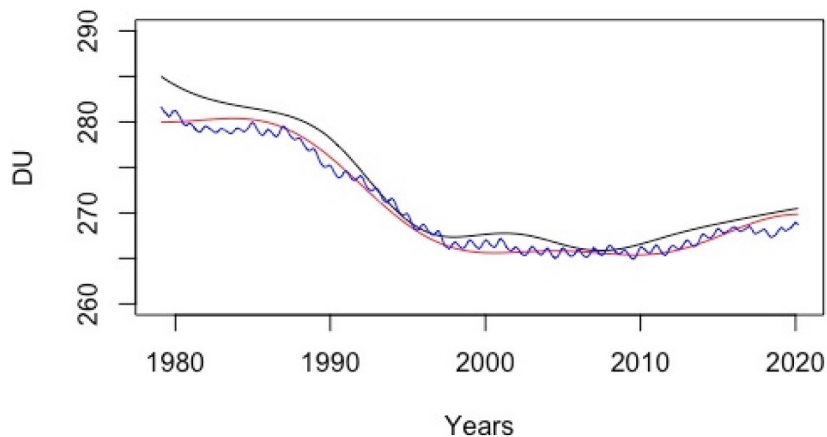
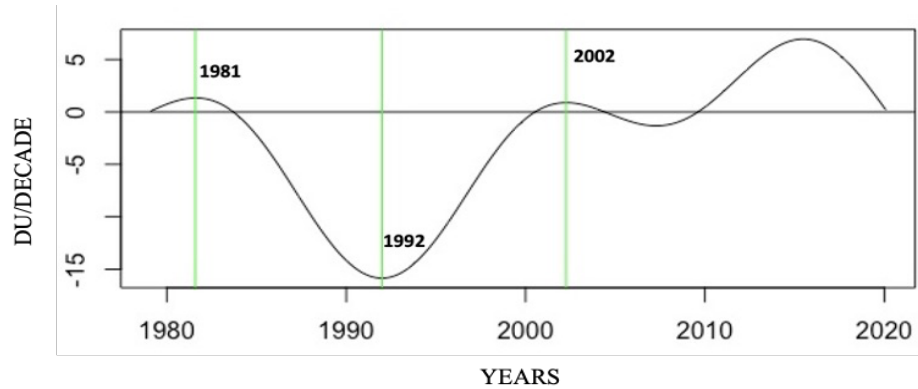


**Figure 11:** The residual  $Trend_{EAWD}$  returned by the EAWD technique (red curve), the trend of the original signal obtained from a moving window (blue curve) having a size fixed at 125 (i.e. 10.4 years), and the residual returned by the EEMD technique (black curve).

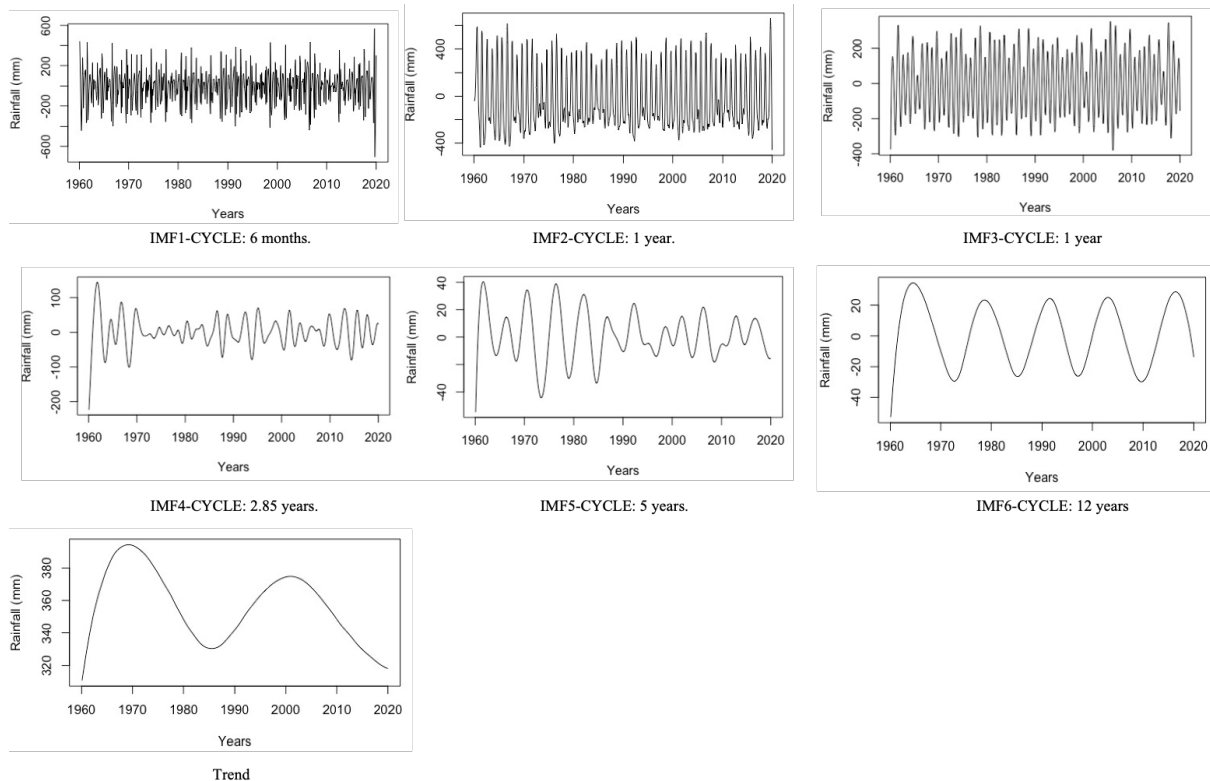
- 1 Likewise, the accuracy of the residual returned by the EAWD technique was estimated using Equation (16):
- 2  $Pr_{EAWD}=0.3\%$ .
- 3 The EAWD trend expressed in DU/decade is shown in the figure below:
- 4



5 **Figure 12:** The DU/decade trend returned by the EAWD technique

- 6
- 7
- 8 Results in Fig. 12 show that ozone levels in Réunion Island decreased from 1981, stopped decreasing in 1992 and started
- 9 rising again from 2002.
- 10 The accuracy of the DU/decade EAWD trend in Fig.12 was calculated as  $2*Pr_{EAWD}$ , i.e., 0.6%.
- 11 EEMD was applied to the rainfall time series measurements and relevant IMFs were selected. Results are
- 12 represented in Figure 13 below.

13



14

- 15 **Figure 13:** Relevant IMFs and Trend from the EEMD applied to Conakry rainfall time-series, from 1960 to 2019.
- 16
- 17 Mode mixing occurs in IMF<sub>2</sub> and IMF<sub>3</sub> as they have the same 1year oscillation cycle. As shown in Figure 15 below,
- 18 frequency  $F_1=1/6$  is contained in both IMF<sub>1</sub> and IMF<sub>2</sub> while  $F_2=1/12$  is contained in IMF<sub>1</sub>, IMF<sub>2</sub>, and IMF<sub>3</sub>.

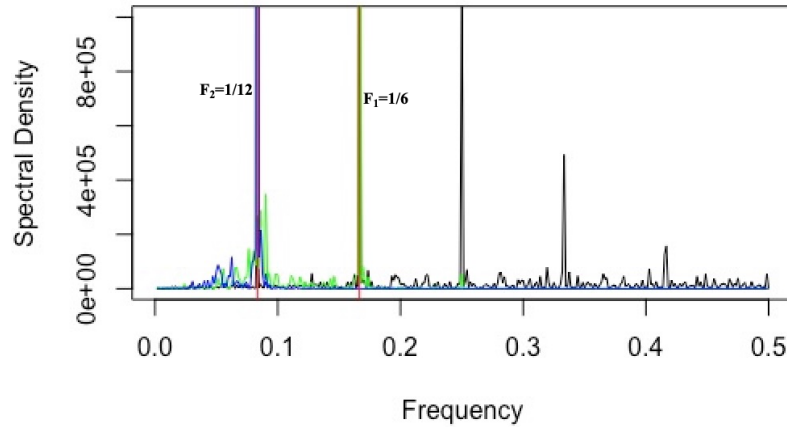


**Figure 15:** Rainfall IMF<sub>1</sub> (black line), IMF<sub>2</sub> (green line) and IMF<sub>3</sub> (blue line) spectral contents.

The accuracy of the trend calculated from EEMD results is compared below with the trend of the original signal obtained from a moving window having its size set at the maximum of the relevant IMFs cycles i.e. 144 months (12 years).

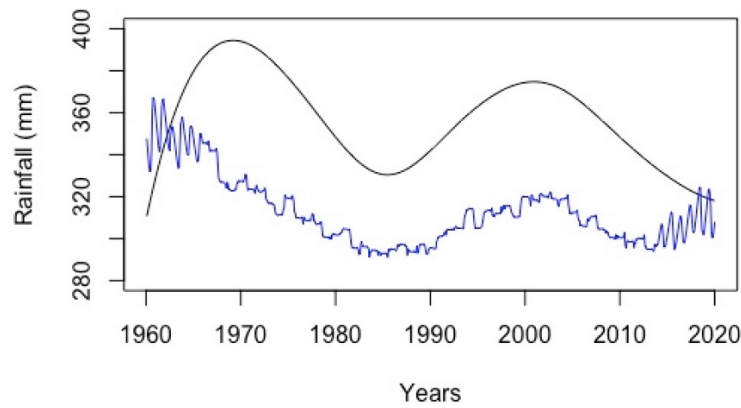


**Figure 16:** Trend obtained from the EEMD technique (black curve) with the trend of the original signal obtained from a moving window (blue curve) with a size of 144 months (i.e. 12 years).

The accuracy of the residual returned by the EEMD technique was estimated using Equation (16):  $Pr_{EEMD}=15\%$ . Results obtained with EAWD are displayed in Figure 17 below.

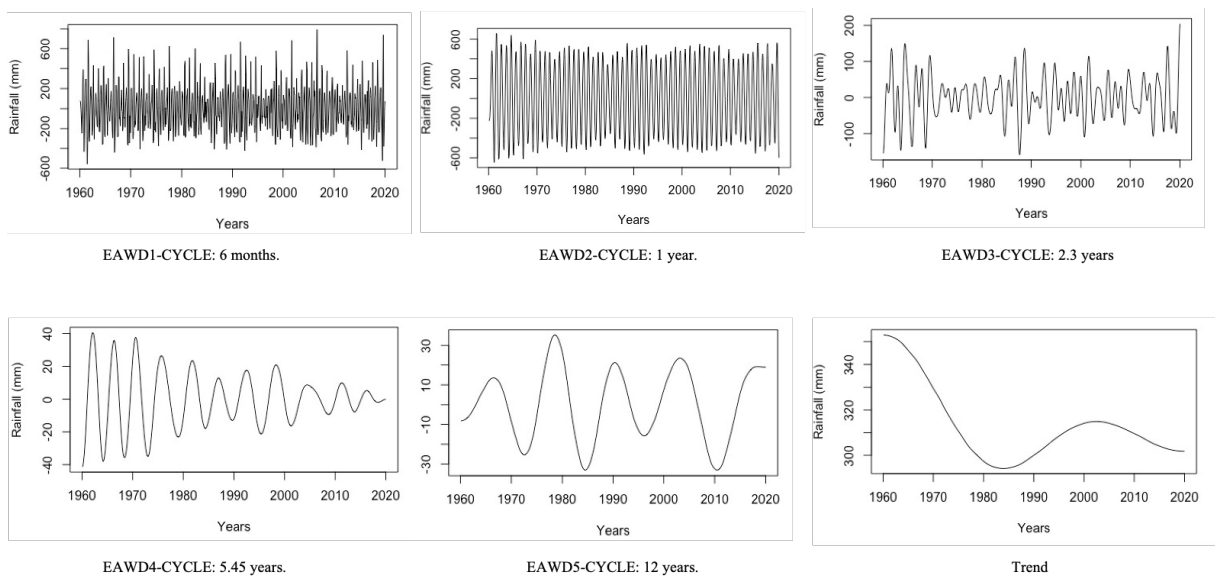
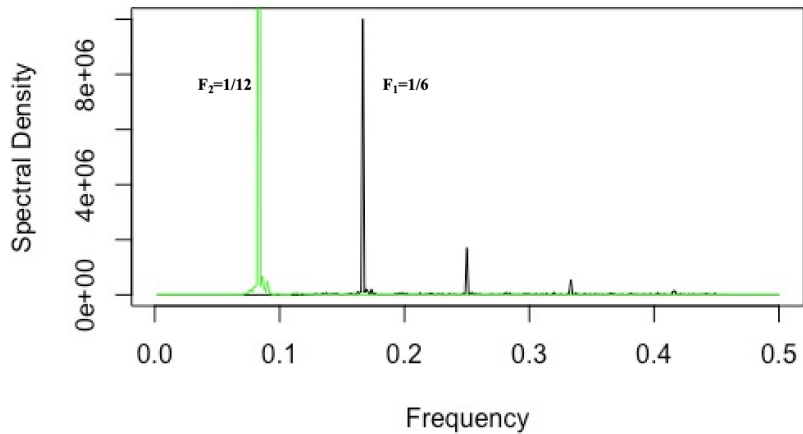


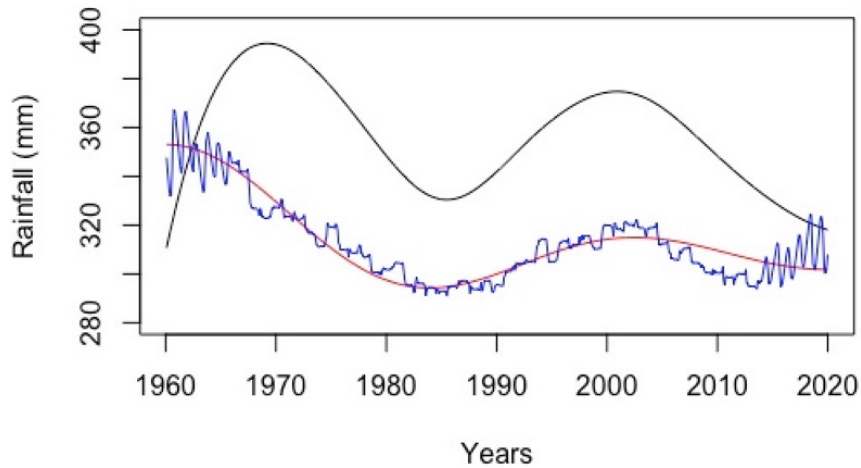
**Figure 17:** Rainfall time-series EAWD decomposition results.

1 The 6 months and 1-year cycles relating respectively to EAWD1 and EAWD2 are correctly separated and the mode mixing  
 2 occurring in the EEMD results has been removed (see Figure 18).



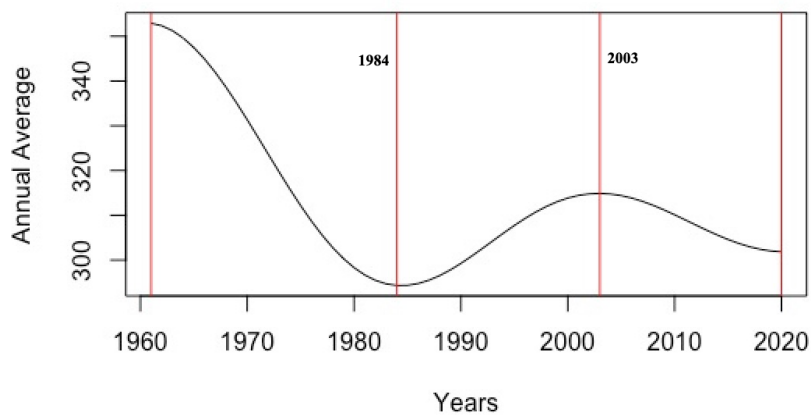
3 **Figure 18:** Rainfall EAWD<sub>1</sub> (black line), EAWD<sub>2</sub> (green line) spectral contents.

4  
 5  
 6 The accuracy of the residual returned by the EAWD technique was estimated at  $P_{TEAWD}=0.9\%$ .



7  
 8  
 9 **Figure 19:** The residual  $Trend_{EAWD}$  returned by the EAWD technique (red curve), the trend of the original signal  
 10 obtained from a moving window (blue curve) having a size fixed at 144 (i.e. 12 years), and the residual returned by the  
 11 EEMD technique (black curve).

12 The EAWD trend represented by an annual average of rainfall (in millimetres) is shown in Figure 20 below.



13  
 14  
 15 **Figure 20:** The EAWD trend as a function of the average rainfall per year

16  
 17 The results reported in Figure 20 show that the rainfall average amount decreased by 2.3 mm per year in the period  
 18 [1960,1984] then increased by 1 mm per year in the period [1984,2003], and decreased again, by 0.7 mm per year, in the  
 19 period [2003,2020].

## 5 Consistency of the EAWD method.

The method commonly employed in atmospheric physics to determine the variability and trend of observation time-series is to use a multilinear regression model. This type of approach has been used very often (Randel and Thompson, 2011; Nair et al., 2013; Bourassa et al., 2014; Gebhardt et al., 2014; Eckert et al., 2014 or Tohir et al., 2018).

The main requirement of this method is the a priori knowledge of the atmospheric climate forcings that control the variability of the time series studied. The ozone-QBO relationship has been discussed in several papers, as has the influence of ENSO on ozone variability (Butchart et al. (2003); Brunner et al. (2006); Randel and Thompson, (2011)). Other papers have shown the role played by solar flux in the temporal variability of ozone (Randel and Wu, 2007).

To validate results obtained with the EAWD method on the TCO time series for La Reunion, we used the multilinear regression model “Trend-Run” developed at the University of Reunion and already applied in many studies (Bencherif et al., 2006; Bègue et al., 2010; Tohir, 2018).

Climate forcings used as input to the TREND-RUN model were QBO, ENSO and solar flux. A linear function was used to estimate the long-term linear trend of the series. The trend was then estimated by calculating the slope of the normalized linear function. As the variability of ozone is also affected by the annual and semi-annual oscillations (AO and SAO), these two analytic oscillations were also used as input to the model. The TREND-RUN model and the climate forcings used (such as ENSO, QBO, solar flux at 10.7 cm) are described in detail in Tohir et al., 2018.

The results obtained here with TREND-RUN on the 1979-2019 La Reunion TCO time-series are consistent with those obtained by Tohir et al., 2018, on a shorter total ozone series at Réunion Island (1998-2013).

The trend obtained from the TREND-RUN model over the whole monthly mean ozone series from 1979 to 2019 is  $-1.11 \pm 0.19$  %/decade. The error is estimated from the standard deviation of the residual found by the model.

The variability components returned by the EAWD method are in agreement with the climatic forcings used as input to the TREND-RUN model and the energy contributions respectively estimated by the TREND-RUN model and the EAWD technique are reported in the table below

IMF	CYCLE	Corresponding proxy used in TREND-RUN model	Energy contribution (%) TREND-RUN	Energy contribution (%) EAWD
1	6 months	SAO	11%	12.2%
2	12 months	AO	66%	58.4%
3	22 months	QBO	3.1%	4.7%
4	45 months	ENSO	0.2%	1.8%
5	125 months	Solar flux	3.6%	3.9%

**Table 1:** Comparison of total ozone variability in Réunion (from 1979 to 2019) obtained with TREND-RUN model and the EAWD method.

The main advantage of the EAWD technique for analysing the ozone variability from an observational time series is that it auto adaptively extracts the modes of variability implicitly contained in the original time series without requiring any a priori knowledge of the atmospheric forcings controlling the ozone variability. It can be seen that the results returned by the EAWD method are in complete agreement with those returned by the TREND-RUN model. On the other hand, the energy contributions of the various modes of variability obtained with the EAWD method are compatible with those obtained with the TREND-RUN method (Table 1).

In contrast to the trend returned by the TREND-RUN model, which is linear over the whole duration of the series, the EAWD technique enables the evolution of the trend to be visualized over the whole period studied.

TREND-RUN has not been applied to the Conakry rainfall time series as it contains intermittent processes, which makes the use of multilinear methods inappropriate.

## 6 Conclusion.

EMD is a method for breaking down a signal without leaving the time domain. It can be compared to other analysis methods, such as Fourier transforms and wavelet decomposition, and the process is very useful for analysing raw signals, which are most often non-linear and non-stationary. Even though the EMD adaptability seems useful for many applications, the major drawbacks with EMD lie in the mode mixing, where the spectral contents of IMFs

1 overlap each other. To overcome this problem, the EWT technique proposes a new approach, introducing a way  
2 of building adaptive wavelets and thus of extracting the different oscillatory modes from a signal by designing an  
3 appropriate filter bank. At the heart of the EWT technique lies the segmentation of the Fourier spectrum of the  
4 original signal. The main idea of the proposed EAWD technique is to use the results provided by EMD to segment  
5 the Fourier spectrum of the original signal. The algorithm implemented uses the spectral contents of the IMFs and  
6 ensures that their supports do not overlap, so that they can constitute a segmentation of the Fourier spectrum of  
7 the original signal. In another way, the method most commonly used to analyse the variability of observation time  
8 series is based on a multilinear regression model. If we look at the results obtained with the TREND-RUN model  
9 on La Réunion TCO time series, the variability modes returned by the EAWD are in good agreement with those  
10 obtained with the multilinear regression model TREND-RUN.

11 From a comparison between the results obtained with the EMD and EAWD techniques, it emerges that the EAWD  
12 technique enables the mode-mixing problem to be overcome while providing a trend with better accuracy than that  
13 obtained with the EMD technique. Thanks to the rigour of the EWT, the EAWD keeps the behaviour of the signal  
14 in the timescales returned by the EMD. In this context, the EAWD technique can be seen as an optimization of the  
15 EMD.

16  
17 This study has been funded by the French National program LEFE.

## 18 19 **References.**

- 20  
21 1- Huang N. E., Z. Shen, S. R. Long, M. C. Wu, H. H. Shih, Q. Zheng, N.- C. Yen, C. C. Tung, and H. H. Liu,  
22 The empirical mode decomposition and the Hilbert spectrum for nonlinear and non-stationary time series  
23 analysis, Proc. of the Royal Society of London A: Math., Physical and Engineering Sciences, vol. 454, no.  
24 1971, pp. 903995, 1998.
- 25 2- Flandrin P., G. Rilling, and P. Gonçalvès, “Empirical Mode Decomposition as a filter bank”, IEEE Sig.  
26 Proc. Soc. Lett, vol 11, no 2, pp 112-114, 2004.
- 27 3- Z.Wu and N. E. Huang, *Ensemble empirical mode decomposition: A noise-assisted data analysis method*,  
28 Adv. Adapt. Data Anal., vol. 1, no. 1, pp. 141, 2009.
- 29 4- Gao Y., G. Ge, Z. Sheng, E. Sang, “Analysis and solution to the mode mixing phenomenon in EMD, IEEE  
30 Congress on image and signal processing, 2008.
- 31 5- Olav B. Fosso, M. Molinas, “Method for mode mixing separation in Empirical Mode decomposition,  
32 arXiv:1709.05547v1 [stat.ME], 16 September 2017.
- 33 6- Delage O., T. Portafaix, H. Bencheriff, G. Guimbretière, R. T. Loua, “Multi-scale Variability Analysis of  
34 Time Series in Geophysics by using the Empirical Mode Decomposition”, Processing SAGA 2019.
- 35 7- Gilles J., “Empirical Wavelet Transform”, IEEE Trans. On Signal Processing, vol. XX, NO XX, February  
36 2013.
- 37 8- Daubechies I., “Ten Lectures on Wavelets”, Society for Industrial and Applied Mathematics, Cbms-Nsf  
38 Regional Conferences Series in Applied Mathematics, 1992.
- 39 9- Wu Z., N.E. Huang, “Ensemble Empirical Mode Decomposition: A Noise-Assisted Data Analysis  
40 Method”, Advances in Adaptive Data Analysis / Vol 01, No 01, PP 1-41, 2009.
- 41 10- Jaffard S., Y. Meyer, R.D Ryan, “Wavelets Tools for Science and Technology”, SIAM 2001.
- 42 11- Meyer Y., “Wavelets, Vibrations and Scaling”, American Mathematical Society, Centre de Recherches  
43 Mathématiques, 1997.
- 44 12- Ayenu-Prah A.Y., N. Attoh-Okine, “A Criterion for Selecting Relevant Intrinsic Mode Functions in  
45 Empirical Mode Decomposition”, Advances in Adaptive Data Analysis, 2010.
- 46 13- Begue N, Bencherif H, Sivakumar V, Kirgis G, Mze N and Leclair de Bellevue J., Temperature variability  
47 and trends in the UT-LS over a sub-tropical site, Reunion, Atmos. Chem. Phys., 10, 8563-8574, 2010.
- 48 14- Bencherif H., R. Diab, T. Portafaix, B. Morel, P. Keckhut, and A. Moorgawa, Temperature climatology  
49 and trend estimates in the UTLS region as observed over a southern subtropical site, Durban, South Africa,  
50 Atmos. Chem. Phys., 6, 5121–5128, 2006.
- 51 15- Tohir, A. M., Portafaix, T., Sivakumar, V., Bencherif, H., Pazmiño, A., and Bègue, N.: Variability and  
52 trend in ozone over the southern tropics and subtropics, Ann. Geophys., 36, 381-404,  
53 <https://doi.org/10.5194/angeo-36-381-2018>,2018.

54